MARK FRICKER

ANALYSIS OF THE ENDOPLASMIC RETICULUM

PLANT SCIENCES, OXFORD
FIRST EDITION

http://www.markfricker.org

PUBLISHED BY PLANT SCIENCES, OXFORD
FIRST EDITION

First printing, June 2016

Current version, August 2016

Contents

1 *Introduction* 5

2 *Installation* 9

3 *Importing images* 13

4 *Profile measurements* 17

5 *Processing images* 19

6 *Analysis of the ER structure* 29

Acknowledgements

The images used in this manual were kindly provided by Verena Kriechbaumer (Oxford Brookes University), and Emily Breeze (University of Warwick). The phase congruency program was written by Peter Kovesi, (Centre for Exploration Targeting at The University of Western Australia). The anisotropic second-order Gaussian kernels were written by Carlos Lopez-Molina (Universidad Pública de Navarra, Pamplona)

1
Introduction

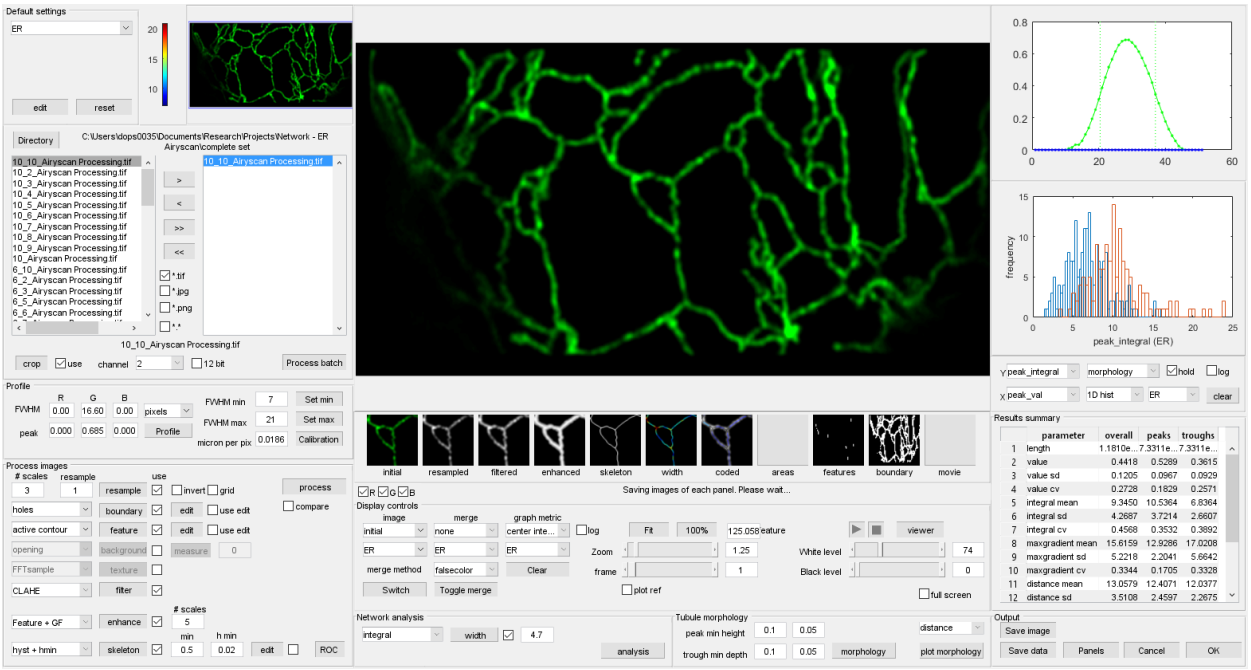

Figure 1.1: The GUI interface for the ER network analysis program

The endoplasmic reticulum (ER) forms a complex and dynamic network of tubules and sheet-like cisternae that ramify throughout the cytoplasm (Fig. 1.5), see Westrate *et. al.* (2015)[1]. The aim of the ER network analysis program is to quantify:

- The length, width and morphology of the ER tubules
- The topological organisation of the network
- The size and shape of the ER cisternae
- The size and shape of the polygonal regions enclosed by the network;

The programs were originally designed to quantify ER organisation in plant epidermal cells, where the ER is confined to a very thin layer of cytoplasm appressed to the periclinal cell wall as a planar, 2-D network. The input image typically comprises single

[1] L. M. Westrate, J. E. Lee, W. A. Prinz, and G. K. Voeltz. Form follows function: The importance of endoplasmic reticulum shape. *Annual Review of Biochemistry*, 84:791–811., 2015

plane (x,y) confocal fluorescence images of ER-targeted fluorescent proteins.

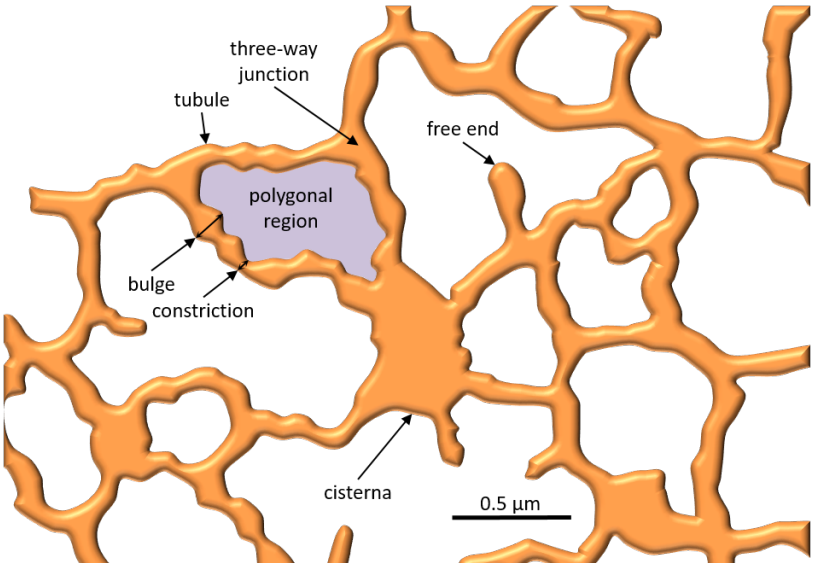

Figure 1.2: Schematic representation of the typical ER morphology

The simplest method to identify the ER automatically would be an intensity-based segmentation of the fluorescent image to give a binary image, with ones representing the ER structure and zeros for the background. However, the resultant binary image is critically dependent on the value for the threshold used, and it is rare that a single threshold provides adequate segmentation without either losing dimmer structures if it is set too high, or artificially expanding and fusing adjacent regions if it is set too low[2]. Thus the approach adopted here exploits additional intensity-independent information over a range of scales and orientations to enhance the network structure, prior to segmentation as a single-pixel wide skeleton (Fig. 1.3).

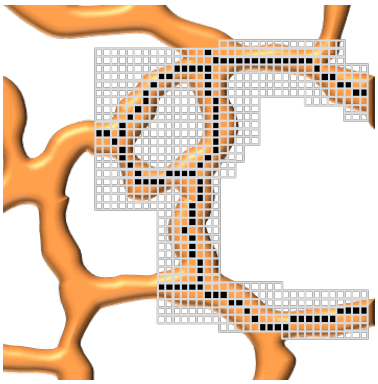

Figure 1.3: Conversion of the ER image to a single-pixel wide skeleton

The expected width of the ER tubule is 50-70 nm (Westrate *et. al.*, 2015), which is below the resolution of the confocal microscope, but can just be resolved with super-resolution techniques, such as stimulated emission depletion microscopy (STED[3]). For most laboratories, access to super-resolution techniques may be limited, necessitating the development of approaches that can be used on a routine basis with existing tools. Thus, the width of the ER can be estimated, even if this is below the resolution limit of the microscope system, with assumptions about the distribution of the fluorescent lumenal marker and the point-spread-function (psf) of the microscope[4]. In this approach, the skeleton is used as a template to interrogate the image locally to provide an estimate of the relative amount of fluorescent probe present, and the width is inferred from the integrated intensity signal. The ER cisternae are typically analysed separately to give measures of their area and shape.

Topological measures of the ER network structure can also be

[2] A.-N. Bouchekhima, L. Frigerio, and M Kirkilionis. Geomteric quantification of the plant endoplasmic reticulum. *J. Microscopy*, 234:158–172, 2009

[3] B. Hein, K. I. Willig, and S. W. Hell. Stimulated emission depletion (sted) nanoscopy of a fluorescent protein-labeled organelle inside a living cell. *PNAS*, 105:14271–14276, 2008

[4] G. J. Streekstra and J. van Pelt. Analysis of tubular structures in three-dimensional confocal images. *Network: Computation in Neural Systems*, 13: 381–395, 2002

extracted following conversion of the pixel skeleton to a weighted, undirected graph, where nodes represent junction points and edges represent the tubules that connect them (Fig. 1.4)[5]. The ER cisternae are represented as a 'super-node' placed at the weighted centroid and connected to all the tubules incident on the boundary. Unlike morphological measurements, the topology of the network is less sensitive to the resolution of the imaging system as it reflects the connectivity of the ER rather than the physical size of the components (Bouchekhima *et al., 2009*).

1.1 *Flow diagram of the main steps in the ER analysis*

The network analysis progresses through a number of parallel threads that are designed to extract different information from the underlying image to characterise the tubular network, cisternae and enclosed polygonal regions. A flow diagram of the overall sequence for morphological measurements is shown in Fig. 1.5.

[5] I. Sparkes, J. Runions, C. Hawes, and L. Griffing. Movement and remodeling of the endoplasmic reticulum in nondividing cells of tobacco leaves. *Plant Cell*, 21:3937–3949, 2009

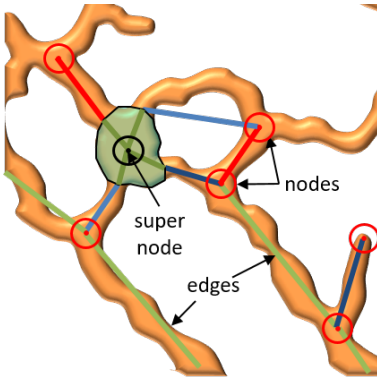

Figure 1.4: Conversion of the ER skeleton to a weighted graph

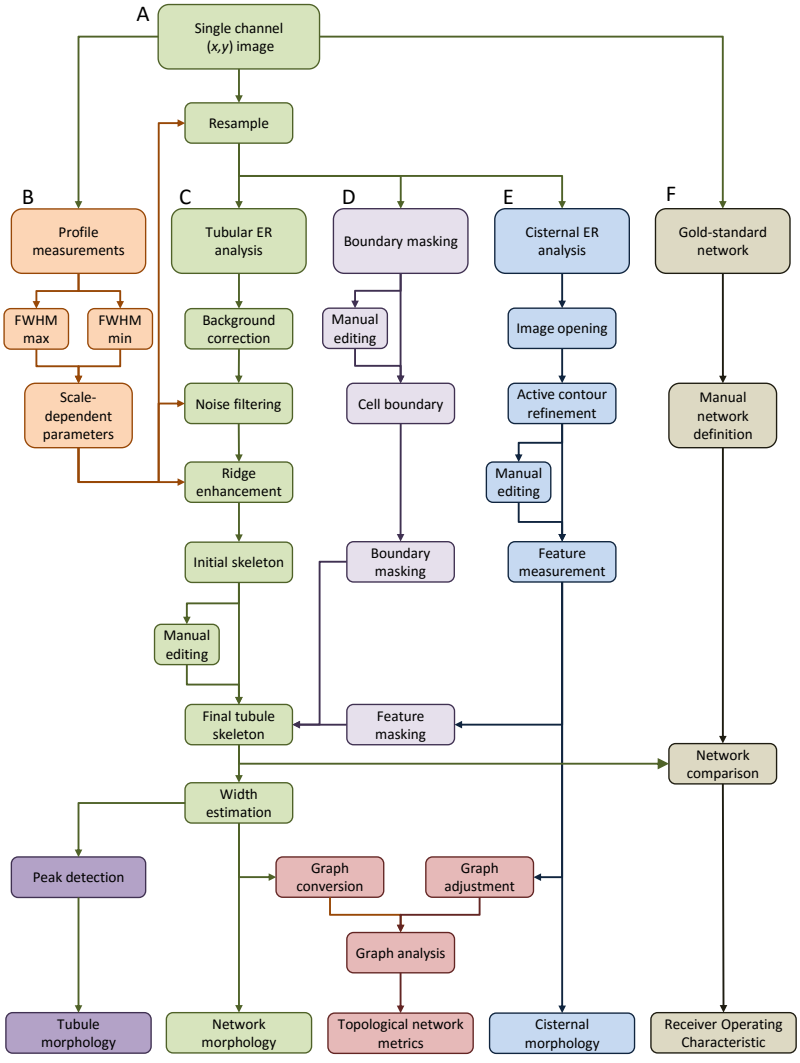

Figure 1.5: A flow diagram showing the main steps in the ER analysis. (A) The starting point is typically a single channel confocal fluorescence of the ER labelled with a fluorescent protein. (B) The minimum and maximum tubule diameters are estimated manually from line transects to resize the image and standardise all the subsequent processing parameters; (C) ER tubules are segmented following filtering and enhancement steps to give a pixel-skeleton. This provides basic morphological information on the length and width of the tubules, and can be interrogated further to examine individual tubule morphology. (D) The analysis can be constrained to a particular cell or sub-cellular region by masking the image; (E) ER cisternae are detected independently using image opening followed by active contour refinement; (F) the performance of the automated segmentation approaches can be compared to a manual gold-standard pixel skeleton

2
Installation

All the programs were written in MATLAB (The Mathworks, Nantick) and are packaged in a single compiled executable file for distribution as a standalone package. The program, manual and tutorial can be downloaded from:

`http://www.markfricker.org`

The software has been tested on Windows10, and requires a minimum screen resolution of 1600 x 900. In addition, an appropriate version of the MATLAB Compiler Runtime (MCR) is required to install the set of shared libraries that enables execution of the compiled MATLAB application. The MCR should automatically download from the MathWorks website when the program is installed for the first time. Alternatively MCR can be downloaded from the MathWorks Website:

`http://www.mathworks.com/products/compiler/mcr`.

Versions are also available as a MATLAB application that runs within the MATLAB 2016a environment and requires the image processing toolbox.

To install the MCR and run the program, double-click the compiled MATLAB self-extracting archive file. This extracts the MATLAB Runtime Installer from the archive, along with all the files that make up the deployed MATLAB environment. Once all the files have been extracted, the MATLAB Runtime Installer starts automatically. When the MATLAB Runtime Installer starts, it displays the following dialog box. Read the information and then click **Next** to proceed with the installation.

Specify the folder in which you want to install the MATLAB runtime in the Folder Selection dialog box and click **Next**.

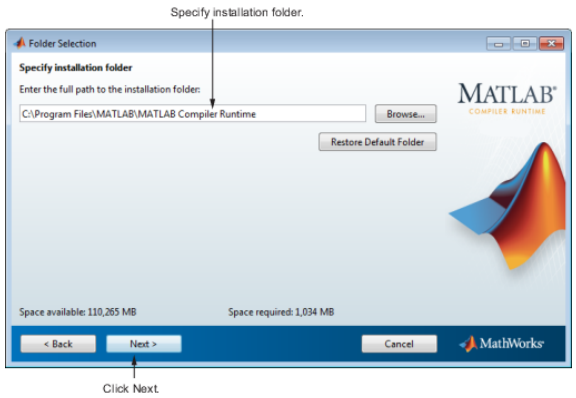

Note: On Windows systems, you can have multiple versions of the MATLAB runtime on your computer but only one installation for any particular version. If you already have an existing installation, the MATLAB runtime Installer does not display the Folder Selection dialog box because you can only overwrite the existing installation in the same folder.

Confirm your choices and click **Install**. The MATLAB Runtime Installer starts copying files into the installation folder

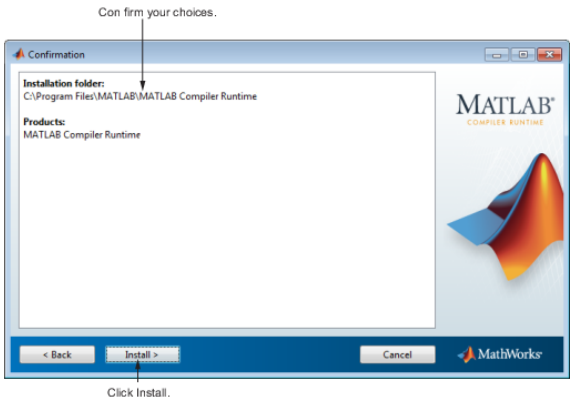

Click **Finish** to exit the installer.

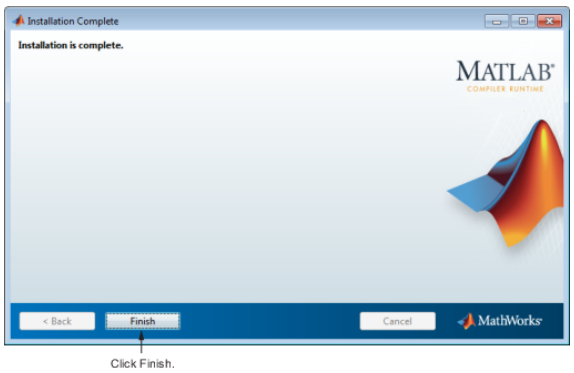

MATLAB Runtime Installer Readme File: A readme.txt file is included with the MATLAB Runtime Installer. This file, visible

when the MATLAB Runtime Installer is expanded, provides more detailed information about the installer and the switches that can be used with it. A number of additional files needed to run the full suite of programs may also be installed at the same time as the main program..

3
Importing images

The ER network GUI automatically displays any image files present in the current directory with the default *.tif extension when the program is started (Fig. 3.1). The working directory can be changed using the **Directory** button, and additional file types can be displayed using the ***.jpg**, ***.png** or ***.*** checkboxes.

A single image can be selected for processing in the left-hand list box using a left mouse-click to highlight the name in the list followed by clicking the **>** arrow. Multiple files in any combination can be selected using *Ctrl + left click* to highlight the files, followed by the **>** arrow. Alternatively, all the files can be selected with the **>>** arrow and will appear in the right-hand list box. Individual files, or all the files can be removed using the **<** and **<<** arrows, respectively.

The default bit depth is 8-bit - if images are saved in 12-bit format, the **12-bit** checkbox needs to be ticked, as the file header will often report that the image is saved in 16-bit format and will not be displayed properly. Once imported, images are normalised to the range 0-1.

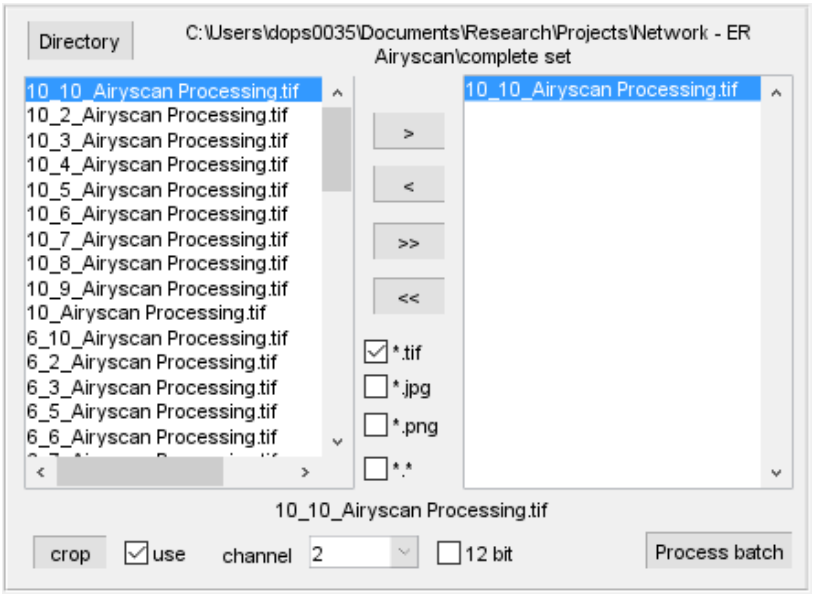

Figure 3.1: Image load panel: Images in standard file formats can be imported, cropped and the relevant channel for processing selected.

The dropdown menu below the list boxloads a set of default processing parameters that are automatically saved in a subdirectory called *parameters* with the filename corresponding to the *"<image filename> _param.mat"*. This parameter file is updated everytime one of the processing or analysis parameters is modified and will be applied the next time the file is loaded.

3.1 *Image display controls*

Once an filename is displayed in the right listbox, the image is automatically displayed in the main window (Fig. 3.2). If multiple files have been selected, the last one in the sequence is shown. Any image can be viewed by clicking on it's filename in the right-hand listbox. At the same time, a thumbnail for the *initial* image is also displayed in the thumbnail shortcut bar immediately underneath the main display. Thumbnails for key steps in the processing sequence are displayed once the appropriate step has completed successfully, and can be used subsequently to switch rapidly between different images.

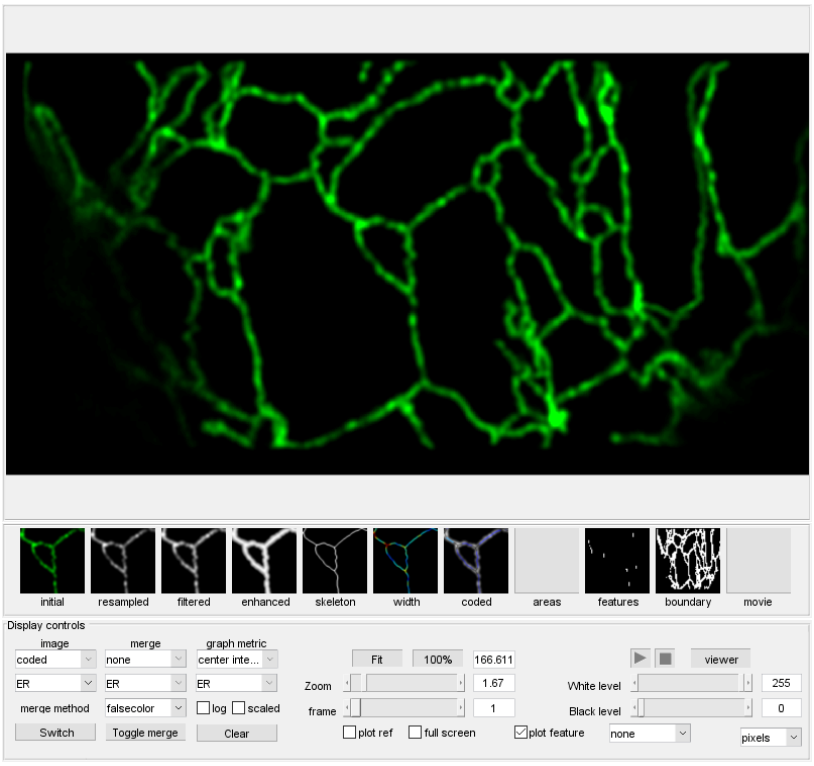

Figure 3.2: Main image display, thumbnail shortcut bar and associated controls to adjust zoom, image contrast and various annotation overlays

A number of options to adjust the image displayed are available in the **Display controls** panel. The main controls that are relevant at this stage adjust the image size and contrast, through the **zoom**, **white level** and **black level** sliders. The **Fit** button resizes the image to ensure all of it is visible, whilst the **100%** button gives a 1:1 image:screen pixel scaling. The other commands in the **Display controls** panel will be covered at a later stage in the manual.

3.2 *Cropping the initial image and selecting the channel*

The **crop** button will automatically show the original image, sized to fill the display window, and prompts the user to drag a rectangle on the image display using the mouse to enclose the desired region-of-interest (ROI). On completion of the rectangle, the image is cropped and the resulting sub-region displayed. If there is an error in the region selected, the process can be repeated by clicking on the filename in the listbox to reload the original image. the co-ordinates of the cropped region are stored in the parameter file associated with the image and will be re-applied everytime the image is loaded if the adjacent **use** checkbox is ticked.

At the moment the software only operates on one channel, which is selected using a dropdown menu underneath the right-hand listbox. To help the user decide on the best channel to process, the checkboxes underneath the **initial** thumbnail can be used to toggle display of the original **R**ed **G**reen and **B**lue channels of the original RGB image .

4
Profile measurements

4.1 Measurement of the approximate tubule diameter

Images of the ER may have been collected at different pixel resolutions, depending on the microscope settings, and may span different width scales depending on the experimental treatment and genetic background. If estimates of the tubule width are required, the pixel size needs to be reduced below the optimal Nyquist sampling value (to 20-30 nm) to reduce downstream discretisation errors due to pixelation.

Figure 4.1: Image profile controls: these allow the user to measure the physical size of structures in the image from transects that automatically calculate the FWHM of the underlying feature. These are used to estimate the minimum and maximum diameters of the tubules to standardise all subsequent processing steps

To standardise all the subsequent processing steps, it is useful to define the expected minimum and maximum width of the tubular components manually using a transect drawn on the image, using the **Set min** and **Set max** buttons in the **Profile** panel (Fig. 4.1).

When either the **Set min** or **Set max** buttons are clicked, the user is prompted to draw a two-point transect on the image across a tubule that, by eye, appears to be close to the smallest or largest tubule diameter, respectively. On completion of the second mouse click, a graph of the transect is displayed in the upper **graph** panel (Fig. 4.2), with the line colour reflecting the intensity values of the original RGB channels.

In addition, the full-width at half-maximum (FWHM) peak intensity is automatically calculated and displayed as:

- two dotted vertical lines on the graph;
- the estimated pixel width in the **FWHM min** and **FWHM max** text boxes, respectively;
- the estimated pixel width and peak intensity (in normalised units) values in the **FWHM** and **peak** text boxes for the **R**,**G** and **B** channels;

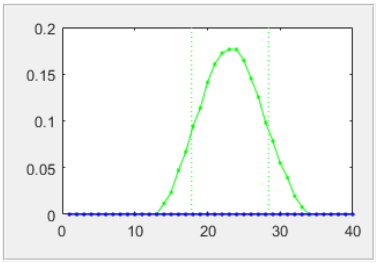

Figure 4.2: Profile measurements: the graph shows the intensity profile along a user-defined transect drawn on the image, along with the full-width half-maximum (FWHM) automatically calculated from the peak height, in this case for the green channel

Values for FWHM are given in pixels, whilst the peak intensity are given in normalised units ranging from 0 to 1. Additional profiles can be drawn at any stage without updating the **FWHM min** and **FWHM max** text boxes by using the **Profile** button.

The value of $FWHM_{min}$ is used to calculate a resampling factor needed to ensure that the minimum apparent tubule width is at least 7 pixels wide to reduce pixelation errors later on. Likewise, $FWHM_{max}$ is used to determine the number of scales to use in the subsequent steps to ensure both that the largest tubules are correctly segmented, and also that structures above this limit are identified as cisternae.

The **Calibration** button prompts the user to define the physical scale between two measurement points on the image, which then updates the adjacent textbox to give the pixel spacing in **micron per pixel**[1]. Alternatively, the pixel size can be entered manually in the text box, if the information is available from the original image file.

[1] Known bug: the *pixels/microns* dropdown menu does not update the pixel values shown in the text boxes to microns.

5
Processing images

5.1 General principles

The **Process images** panel contains the controls needed to convert the original image file to a binary pixel skeleton of the ER (Fig. 5.1).

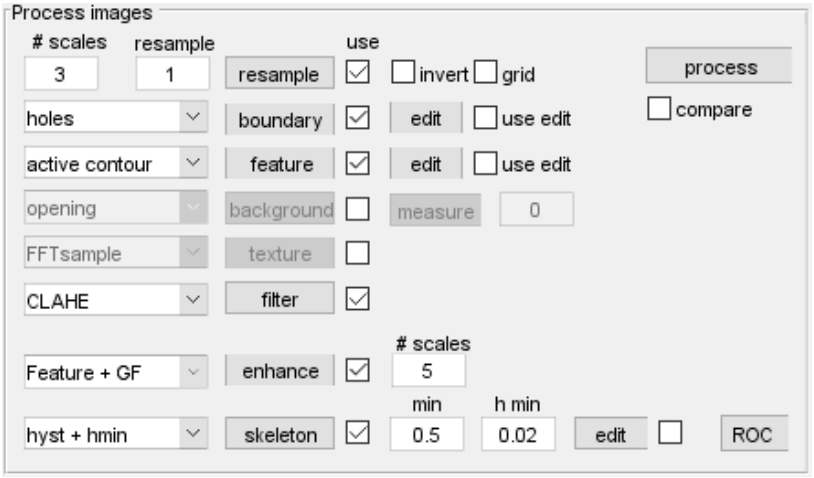

Figure 5.1: Image processing panel: These controls set the parameters for the main processing steps to extract a binary pixel skeleton from the initial image

Each step has a number of options that can be selected from the adjacent dropdown menu on the left. In addition, some steps allow the user to manually modify the image produced at a particular step, or to set the values for specific parameters. The **use** checkboxes enable the user to toggle particular steps on or off to explore the impact on the final skeleton. If a particular step is not operational, the corresponding controls are greyed-out. The **process** button runs the entire sequence of steps on the currently selected image.

The **Process Batch** button in the **Image Load** panel runs the complete process and analysis sections for every selected file and also automatically saves the data and images.

The **ROC** button allows comparison with the automatically extracted pixel skeleton and a hand-drawn gold-standard reference.

5.2 *Image resampling*

The values of $FWHM_{min}$ estimated from the **Profile** measurements is automatically used to calculate the resampling factor needed to ensure that the minimum tubule is at least 7 pixels wide. Likewise, the $FWHM_{max}$ value is used to determine the number of scales to use in the subsequent steps to ensure both that the largest tubules are correctly segmented, and also that structures above this limit are identified as cisternae.The resample **use** checkbox is active by default. If the box is unchecked, no resampling takes place, but it is possible that subsequent steps do not perform as expected. Once the **resample** button is clicked, the initial image is resampled and displayed. The *resample* thumbnail is updated to show a small icon taken from the center of the resampled image.

5.3 *Setting up a boundary mask*

In some instances it may be appropriate to define a boundary mask to exclude regions that should not be analysed, or to restrict the analysis to a specific region of the cell or tissue. The default setting is not to use a boundary, but ticking the boundary **use** checkbox will enable the boundary controls.

The adjacent dropdown menu provides a number of options including:

- *'Holes'* : this segments the main fluorescent structures using an automatic threshold determined by Otsu's method[1] (that minimizes the intraclass variance of the foreground and background distributions), but does not fill in any gaps or holes in the resulting binary image. Care is needed with this step as the thresholding operation may introduce breaks in some dim tubules, which are then not considered in subsequent processing steps.
- *'No holes'* : follows the same approach as the *'holes'* option, but also fills any internal holes in the binary image.
- *Background* : prompts the user to define a ROI in a background area of the image. The threshold is then calculated as the $background\ mean + 2 * SD\ units$.

[1] N. Otsu. A threshold selection method from gray-level histograms. *IEEE Trans. Systems, Man, Cyber.*, 9:62–66, 1979

Clicking the **Boundary** button runs the chosen method, displays the segmented binary image alongside the initial grayscale image to aid comparison, and updates the boundary thumbnail (Fig. 5.2)[2].

It is possible that the automatic boundary settings do not provide the desired masking of unwanted information, requiring the user to define the mask manually. The **edit** button will open an additional window with a set of tools to allow manual adjustment of the binary image. Full details of the binary editing program are given in Chapter **??**. If a boundary image has been defined manually, the **use edit** checkbox is automatically activated and

[2] Care is needed with this step as the automatic thresholding operations may introduce breaks in some dim tubules, which are then not then available for consideration in subsequent processing and analysis steps

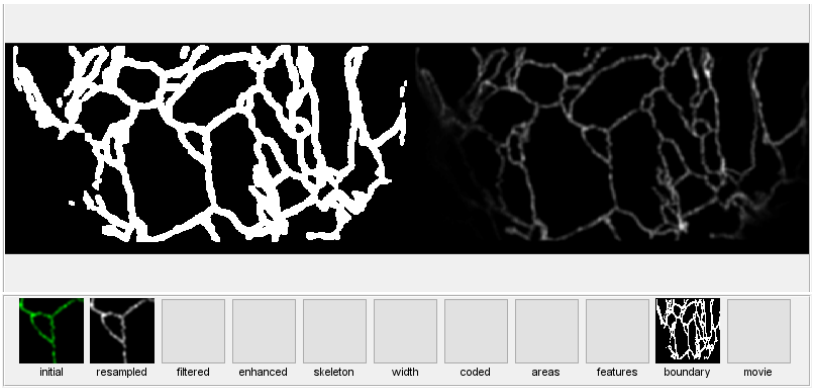

Figure 5.2: Side-by-side display of the boundary segmentation image using the 'holes' option. The boundary thumbnail is also updated

the manually defined boundary will be applied to subsequent processing steps.

5.4 *Defining additional image features such as ER cisternae*

In addition to the tubular-reticulum, the ER may also include sheet-like regions called cisternae, or regions of closely appressed tubules that are difficult to separate. The methods used to segment the tubular ER do not work with the cisternae, so a different set of controls are available to allow the user to segment these structures independently. To enable the **Feature** controls , the feature **use** checkbox needs to be ticked. The adjacent dropdown menu then gives access to several different methods including:

- *'Auto'* : Automatic segmentation using an intensity-based threshold to pick out the brightest structures. An automatic multi-threshold is used to partition pixel intensities into three bins, and the upper bin selected. This will extract the brightest objects, but it does not usually give a good unique segmentation of cisternae.
- *'Opening'* : Uses image opening to calculate a modified image after grayscale opening to remove all objects smaller than $FWHM_{max}$, and then converts the resultant image to a binary mask using an automatic threshold. This is more effective at detecting larger sheet-like regions of the ER, but the resultant binary image tends to give blob like features that extend beyond the original cisternal regions.
- *'Active contour'* : Performs the same image opening step as 2 above, but then 'shrinks' the features detected down to match the underlying intensity profile using an active contour algorithm. This often performs better than a simple opening operation and is set as the default..

Clicking the **Feature** button runs the chosen method, updates the feature thumbnail and displays the segmented binary image superimposed on the initial grayscale image in falsecolour (Fig. 5.3 (a)). Once the features have been defined, the **plot feature**

checkbox in the **display** panel will superimpose the outline on any displayed image in a red-and-white border (Fig. 5.3 (b)). A number of morphology measurements of the cisternae are provided including the area, major and minor axis lengths, perimeter and solidity.

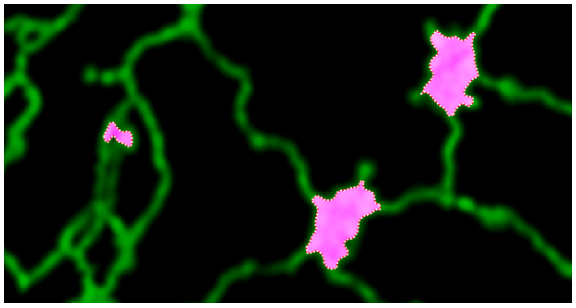

(a) Detection of ER cisternae and appressed tubues

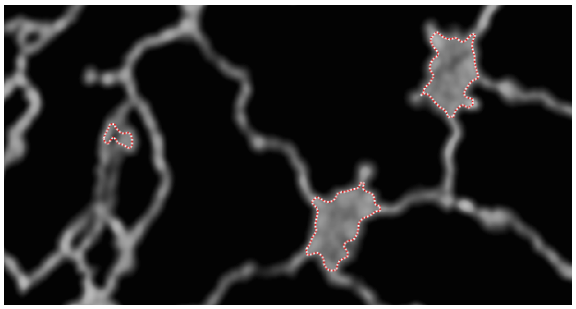

(b) Feature boundaries

*Figure 5.3: Feature detection: (a) False-colour merge of the features segmented using image opening and active contours that highlight ER cisternae or dense regions of appressed tubules. (b) The resulting feature boundary can be superimposed on any underlying image using the **plot feature** checkbox*

If no satisfactory segmentation of the features can be achieved with the automatic settings, the feature **edit** button opens the binary editing window to allow manual adjustment of the binary image. Full details of the binary editing program are given in Chapter **??**. If a feature image has been defined manually, the **use edit** checkbox is automatically activated and the manually defined features will be used in subsequent processing steps.

5.5 *Background measurement and correction*

Accurate measurements of the fluorescence signal from the ER requires correction for instrument dark current, amplifier offset and background signal. The **Background** checkbox activates a number of options to automatically or manually correct the background contribution including:

- *'Subtract'* : This will subtract a constant value from the image and is appropriate for removing instrument black-level offsets or very diffuse fluorescence. The *value* is set in the adjacent text box and can be input manually, or measured using the **measure** button which prompts the user to define a background ROI on the image for the measurement.
- '*Opening'* : the image is processed with an opening function using a disk-shaped kernel with the radius set by **FWHM max**

/ **resample** (i.e. twice the size of the largest feature expected). This removes any features smaller than $2 * FWHM_{max}$ and provides an estimate of the local background around each pixel. The opened image is subtracted from the original to correct for the local background. This method may be useful if there is some out-of-focus blur in the image or an amount of signal from another compartment, such as the cytoplasm. However, it is less useful if there are large sheet-like regions larger than $2 * FWHM_{max}$, as these remain after the opening operation and are then subtracted from the image, distorting the pixel intensities in the neighbouring regions.

- *'Surface fit'* : this finds all the local minima across the image and fits a surface to points in the 10-90% interval. The surface is converted to an image and subtracted from the original.
- *'Sub low pass'* : the image is filtered using a Gaussian kernel with a large radius sufficient to remove all the high-frequency information in the image. The standard deviation for the Gaussian kernel is calculated as $FWHM_{max}$, or approximately twice the size of the largest tubule diameter. The low pass image is subtracted from the original and the image re-normalised.

5.6 Filtering the image to improve signal-to-noise

Most simple noise reduction algorithms use isotropic kernels and smooth the noise in the image equally in all directions. This is not desirable when analysing the ER, as the tubule boundaries will become blurred. Instead a number of adaptive anisotropic filters are provided that smooth within the tubular network structures, but do not spread across boundaries. In addition, the image intensities can subsequently be rescaled using local contrast-limited adaptive histogram equalisation (CLAHE).

The first set of options (shown as **texture**) are not usually required for analysis of the ER. These options are intended to remove regions with specific frequency components in structures that fall outside the range expected for the target structures.

The **filter** controls can be used to locally smooth the image with various adaptive filters, and/or increase the contrast using contrast-limited adaptive histogram equalisation (CLAHE). The current options include:

- *'CLAHE'* : applies contrast-limited adaptive histogram equalisation[3] to the image to expand the contrast range over local regions.
- *'Coherence'* : applies an anisotropic diffusion filter written by Dirk-Jan Kroon[4] that smooths regions of low variance, but avoids blurring of object boundaries.
- *'Guided'* : applies an edge-preserving smoothing filter that is guided by the intensities in the original image[5]

[3] K. Zuiderveld. *Contrast limited adaptive histograph equalization*, pages 474–485. Graphic Gems IV. Academic Press Professional, San Diego:, 1994

[4] D. J. Kroon, C. H. Slump, and T. J. Maal. Optimized anisotropic rotational invariant diffusion scheme on cone-beam ct. *Med Image Comput Comput Assist Interv*, 13:221–8, 2010

[5] K. He, J. Sun, and X. Tang. Guided image filtering. *IEEE Transactions on Pattern Analysis and Machine Intelligence*, 35:1397–1409, 2013

- *'Coherence + CLAHE'* : applies the *'Coherence'* filter followed by histogram equalisation.
- *'Guided + CLAHE'* : applies the *'Guided'* filter followed by histogram equalisation.

The filtering and contrast adjustment are applied to aid segmentation of the pixel skeleton. Quantitative measurements always refer back to the original image intensities CLAHE is only needed if the subsequent segmentation step is dependent on image intensities, although visually it helps the user see detail across the whole image.

5.7 Enhancing the tubular elements

A number of options can be used to improve the relative contrast of tubular ER elements prior to segmentation using kernels designed to pick-out âĂŸridgeâĂŹ like features that are applied over a range of scales and angles. These include:

- *'Feature Type'* : Uses the phase-congruency approach developed by Peter Kovesi[6,7] which provides contrast-invariant ridge detection over a range of scales and angles. The MATLAB implementation[8] provides a number of outputs, including the level of phase congruency as a measure of the edge strength (Fig. 5.4 (a)), but also the feature type, calculated as the weighted mean phase angle at every point in the image (Fig. 5.4 (b)). A value for the feature type of $pi/2$ corresponds to a bright line, 0 corresponds to a step and $-pi/2$ is a dark line. The feature type has proved to be one of the most robust and reliable outputs for subsequent segmentation, as all ridges, irrespective of their original intensity are identified with equal strength in the feature type image (Fig. 5.4 (b)).
- *'Feature + CF'* : This applies the Kovesi phase congruency enhancement and subsequently filters the feature type image with a *'Coherence'* filter to smooth small discontinuities near some junctions.
- *'Feature + GF'* : Applies the Kovesi phase congruency enhancement with a subsequent *'Guided'* filter.
- *'Frangi'* : This calls the Matlab implementation of the classic Frangi[9] 'vesselness' filter written by Marc Schrijver and Dirk-Jan Kroon and available from the Mathworks website (Fig. 5.4 (c)). This gives a strong response for bright features where the second-order derivative of the image (Hessian) shows a strong anisotropy.
- *'Ridge'* : Applies a version of the second-order anisotropic Gaussian kernel originally proposed by Meijering *et al.* (2004)[10] as part of their 'Neuriteness' detector. This uses a slightly flattened

[6] P. Kovesi. Image features from phase congruency. *Videre: Journal of Computer Vision Research*, 1(3):1–26, 1999

[7] P. Kovesi. Phase congruency: A low-level image invariant. *Psychological Research*, 64:136–148., 2000a

[8] P. D. Kovesi. MATLAB and Octave functions for computer vision and image processing, 2000b. Available from: http://www.peterkovesi.com/matlabfns/

[9] A. Frangi, W. Niessen, K. Vincken, and M. Viergever. Multiscale vessel enhancement filtering. *Medical Image Computing and Computer-Assisted Interventation*, 1496:130Ű137, 1998

[10] E. Meijering, M. Jacob, J. Sarria, P. Steiner, H. Hirling, and M Unser. Design and validation of a tool for neurite tracing and analysis in fluorescence microscopy images. *Cytometry*, 58A:167Ű176, 2004

second-order Gaussian kernel at a range of scales and angles to give better discrimination of ridge-like structures, but does not include any additional information related to the anisotropy of the ridges.

- *'Lopez-Molina'* : Applies the multi-scale ridge detector developed by Lopez-Molina *et al.* (2015)[11] that uses anisotropic second-order Gaussian kernels. These can be configured flexibly in terms of size, orientation and anisotropy. This gives good ridge enhancement, but still retains the variation in local intensity along the tubules that can make subsequent segmentation more difficult. (Fig. 5.4 (d)).

[11] C. Lopez-Molina, G. V. D. de Ulzurrun, J. M. Baetens, J. Van den Bulcke, and B. De Baets. Unsupervised ridge detection using second order anisotropic gaussian kernels. *Signal Processing*, 116:55–67, 2015

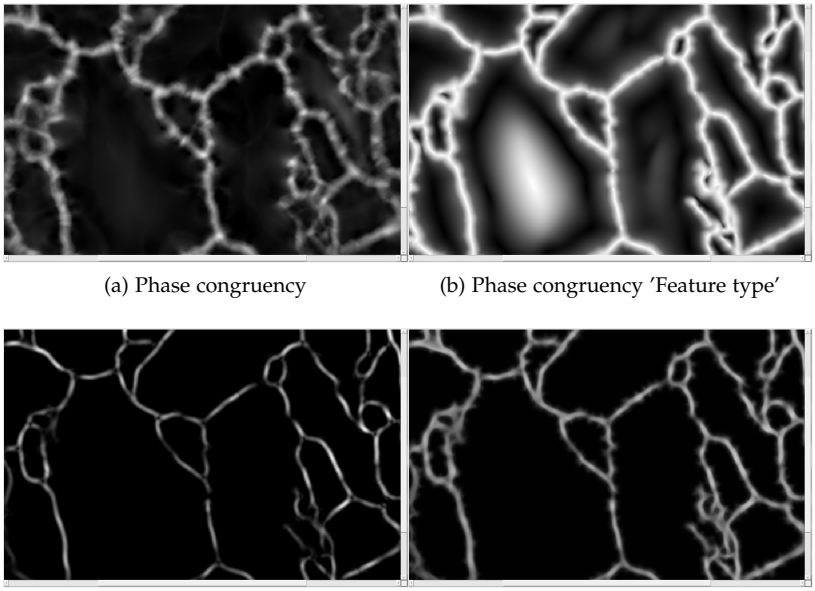

(a) Phase congruency (b) Phase congruency 'Feature type'

(c) isotropic second-order Gaussian (d) anisotropic second-order Gaussian

Figure 5.4: Comparison of different multi-scale approaches to ridge enhancement. (a) the raw output of the phase congruency as an intensity-independent measure of ridge strength (Kovesi, 1999,2000a,b); (b) the feature type output of the phase congruency method. Note the strong edge response irrespective of the original tubule intensity; (c) the classic Frangi et al. (1998) algorithm based on the asymmetry of the isotropic second-order image gradient (note the 'gaps' that appear at the tubule junctions); (d) the output of anisotropic second-order Gaussian filters according to Lopez-Molina et al. (2015)

In each case the number of scales is initially set by the # *scales* parameter, determined from the ratio of $FWHM_{max}/FWHM_{min}$, with a minimum bound of 3. However, this can be over-ridden using the adjacent textbox. This may be necessary to ensure that larger features, such as cisternae, are also processed prior to segmentation. The number of orientations is fixed at 6. In the case of the anisotropic Lopez-Molina filters, the anisotropy is set at 1.3.

5.8 Skeletonization

The aim of the skeletonization step is to convert the enhanced image (Fig. 5.4 (a)) to a one-pixel wide skeleton along the centre-line of the tubule ridges. This is only an approximation to the true centre-line due to the pixel discretisation errors. There are two main approaches that can be used, namely âĂŸhysteresis thresholding', that uses intensity information and some degree of pixel connectivity to provide an initial binary image that then has to be thinned to give a single pixel skeleton, and 'watershed

thresholdingâĂŹ which follows connected ridges, irrespective of the absolute intensity and automatically generates a single pixel skeleton.

- *'Hysteresis thresholding'*, that is based on intensity information and some degree of pixel connectivity (Fig. 5.4 (b));
- *'watershed threshold'*, that follows connected ridges, irrespective of the absolute intensity (Fig. 5.4 (c,d)).

The watershed is better at segmenting the centre-line of the ridges and can handle variations in intensity well. However, it does not include any tubules that have a free end, and has a tendency to over-segment regions with noise (e.g. Fig. 5.4 (c)). Over-segmentation can be avoided by including additional steps that suppress regions with small intensity fluctuations, and also to impose local minima to ensure adjacent structures are resolved (Fig. 5.4 (d)).

Hysteresis thresholding starts with seed pixels above the upper threshold, and then propagates the initial segmentation as long as pixels remain above the lower threshold. The resulting binary image is then thinned to give the single-pixel skeleton. The value of the lower threshold is critical - too high and the network becomes disconnected; too low and large blocks of the image are included in the resultant binary image that may fuse separate tubules into a single object. When this block is thinned, the skeleton does not map onto the ridge centre-lines. In addition, as the thinning process is not guided by the intensities in the enhanced image, the skeleton does not necessarily converge on the expected pattern at junction points. These various options are selected from the drop down menu as follows:

- *'Hysteresis'* : applies hysteresis thresholding using a lower threshold set by the adjacent textbox. The upper threshold used to define the seed points is automatically set as $lower\ threshold + 0.2$ 5.4 (b)).
- *'Watershed'* : applies a watershed segmentation and then extracts the watershed lines as the pixel skeleton. 5.4 (c)).
- *'Hist + hmin'* : applies an h-minimum transform to smooth out regions with low fluctuations in intensity, but then sets these regions as local minima to ensure that the surrounding ridges will be segmented individually and do not spread into the basin, even if the absolute values are above the lower hysteresis threshold.
- *'WS + hmin'* : uses the same h-minimum transform and imposes local minima before the watershed operation, to prevent over-segmentation of irrelevant ridges arising from noise within the basins 5.4 (d)).

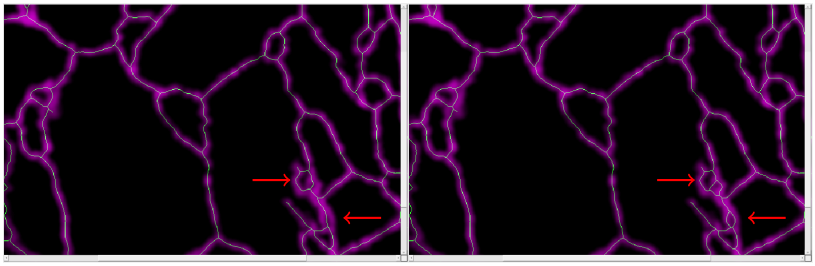

(a) Overlay of pixel skeleton using hysteresis thesholding

(b) Improvement in the pixel-skeleton with inclusion of the h-minimum transform

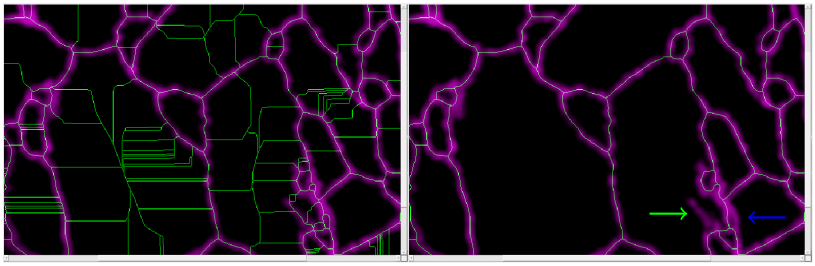

(c) Over-segmentation using an unconstrained watershed segmentation

(d) Pixel skeleton following a constrained watershed segmentation

Figure 5.5: Comparison of different approaches to extraction of the pixel skeleton. (a) segmentation using hysteresis thresholding. Note that some adjacent regions are not separated and the skeleton crosses the void between the tubules (red arrows); (b) Improvement in segmentation following an h-minimum transform and imposing a local minimum. The adjacent tubules are now correctly segmented; (c) segmentation using an unconstrained watershed. This over-segments regions of background, that still have almost invisible ridge lines in the noise; (d) suppression of watershed over-segmentation using the h-minimum transform and imposed local minima. Note that the free tubule (green arrow) is lost in the watershed segmentation, and some arms of the loops are lost (blue arrow)

5.9 Modifying the skeleton to accommodate ER cisternae

The initial pixel skeleton will include both tubular and cisternal regions, even though a 'skeleton' is not necessarily a good representation of the cisternal morphology. If the cisternal features have been segmented earlier in the sequence, these regions are punched out of the pixel skeleton so that they do not contribute to analysis of the tubular elements. During the analysis steps, described in (Chapter)6), the cisternal regions are represented as a set of linear connections radiating out from the center to connect with the tubules incident on the boundary. This ensures the overall connectivity of the network is retained.

5.10 Manual editing of the pixel skeleton

If the automated methods to delineate the pixel skeleton are still incorrect, the skeleton can be edited manually using the **edit** button. This opens the binary editing program described in Chapter ??

6
Analysis of the ER structure

6.1 Estimation of the tubule diameter

Once the pixel-skeleton has been segmented satisfactorily, the first step in the analysis is to estimate the tubule width. Unfortunately, the average ER tubule diameter (50 nm) is below the theoretical resolution of most confocal microscopes and at the resolution of current live-cell super-resolution techniques such as STED[1], so direct physical estimates of the width are challenging. The methods described here typically return a value of the true width convolved with the point spread function (psf) of the microscope. In addition, the typical pixel spacing leads to significant digitisation errors, even with over-sampling. A number of different approaches are available that all provide some information on the tubule diameter including:

[1] B. Hein, K. I. Willig, and S. W. Hell. Stimulated emission depletion (sted) nanoscopy of a fluorescent protein-labeled organelle inside a living cell. *PNAS*, 105:14271–14276, 2008

- *'Distance'* : This estimates the local FWHM from the original tubule intensity for each pixel in the skeleton. The peak height is estimated from the original intensity, whilst the distance is estimated from the distance transform of the pixel skeleton. The 50% threshold is estimated from where the pixel intensity falls below half the peak intensity, assuming a local background of zero.

- *'Maximum-gradient granulometry'* : The intensity image is subject to a series of image openings (erosion followed by dilation) that successively remove structures as the size of the opening kernel exceeds the underlying object. This results in an intermediate (x,y,s) image, where s increases with the size of the disk-shaped kernel. The intensity of each pixel initially decreases slowly with s as the kernel samples more of the object, but then reduces dramatically once the boundary of the object is reached, and the kernel only samples the background. The transition point for any pixel is determined from the maximum (negative) gradient of the granulometry curve. This approach constrains the width to integer pixels values, and also suffers from the digital approximation of small kernels to a true disk shaped kernel.

- *'Integrated intensity granulometry'* : This approach follows the same methodology as the maximum-gradient granulometry

method, but rather than extract a specific size threshold, the integrated intensity under the granulometry curve is calculated. An additional option is available to use the $FWHM_{max} + 1$ kernel as a local background correction. This provides a more nuanced interrogation of the local image intensity, but cannot be directly related to the physical tubule width without additional assumptions about the relationship between fluorescence intensity and sampled volume. Nevertheless, this approach does help with estimation of relative tubule widths, even if they are sub-resolution objects, provided it is assumed that the fluorescent probe is evenly distributed throughout the ER, and the ER is within the sampling volume of the confocal defined by the psf. The textbox adjacent to the **width** button can be used to input a conversion factor to convert relative fluorescence to width if it is possible to correlate between physical width and intensity, measured using the **Profile** controls (4). We have found that the simplest way to estimate the empirical intensity calibration factor is to take the average intensity for a cisternal sheet (using the profile tool). Typically this is about 0.3-0.5, and represents the signal expected for a sheet-like structure completely filling the (*x*,*y*) plane of the psf with the same thickness as the tubules.

This principle behind the integrated intensity measurements can be illustrated empirically using a simulated model of ER tubules with different widths (Fig. 6.1A,B) that are convolved with the excitation and emission psfs, modelled as anisotropic 3-D Gaussian[2] blurring functions (Fig. 6.1C,D).

[2] B. Zhang, J. Zerubia, and J.-C. (2007). Olivo-Marin. Gaussian approximations of fluorescence microscope point-spread function models. *Applied Optics*, 46:1819–1829, 2007

The performance of the three different width estimators can be assessed by analysis of a single confocal plane to represent a single (x,y) image (Fig. 6.1E), and shows That all measures perform well above about twice the theoretical lateral FWHM of the psf (0.14 μ m for the Zeiss AiryScan), but the 50% distance measure and the maximum-gradient granulometry measure both converge to a fixed value close to the psf for sub-resolution objects as expected (Fig. 6.1G). By contrast, the integrated intensity measure provides near linear performance even with sub-resolution objects (Fig. 6.1G). An additional option is available to increase the speed of the granulometry by using decomposition of the disk-shaped structuring element into a set of linear elements. This requires an empirically determined correction of -1 pixel to the estimated width to compensate for the over-sampling with essentially square kernel approximations (Fig. 6.1H).

All three width estimates are calculated automatically by clicking the **width** button. The only user option required is to select whether the *'integral'* approach also includes subtraction of the last + 1 image following image opening to remove the local background. For most fluorescence images this is not really necessary unless there is significant background or blur. The width is presented as a pseudo-colour coded version of the pixel skeleton that is scaled

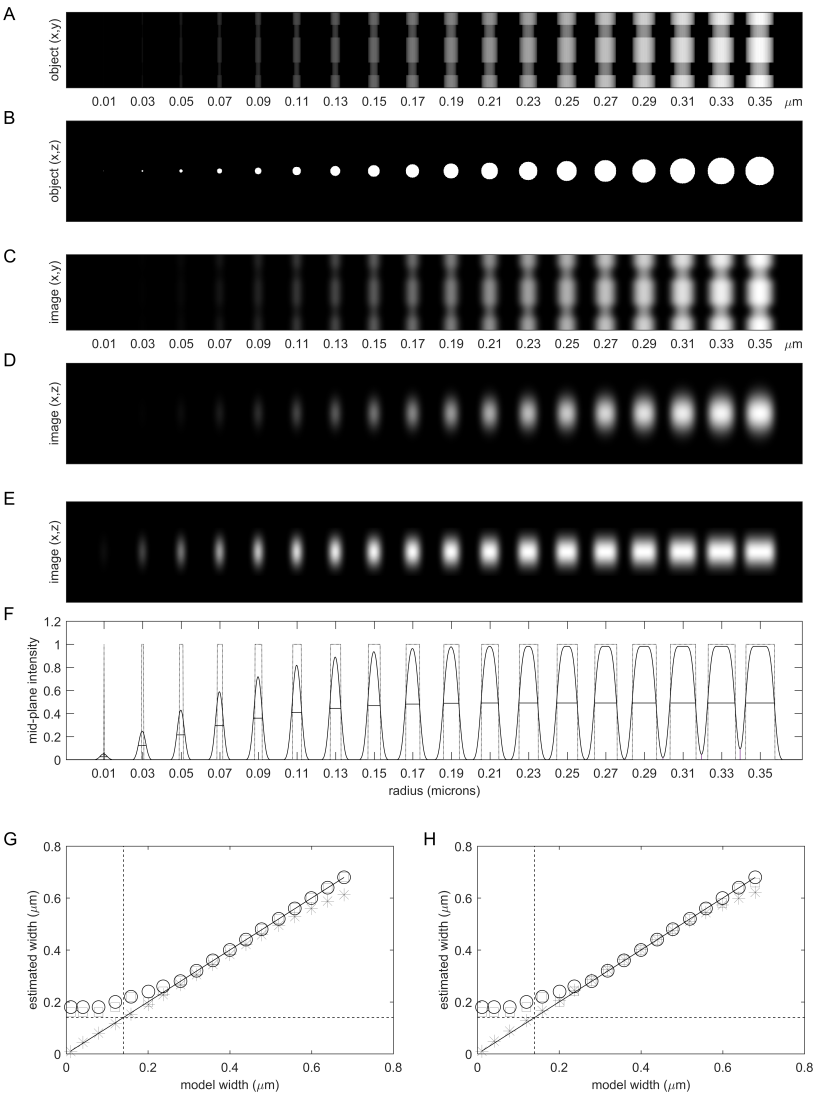

Figure 6.1: Estimation of sub-resolution tubule widths. A set of ER tubules with increasing width were simulated as cylinders and viewed as an average (x,y) projection (A,C) and a single (x,z) section (B,D) before (A,B) and after (C,D) blurring with a simulated anisotropic 3-D Gaussian excitation and emission point spread function (FWHM $0.14\mu m \times 0.14\mu m \times 0.42\mu m$ in x,y and z, respectively). The simulated result for scanning a single confocal section is illustrated in (E). The intensity profile across the mid-section of the original tubules and after blurring is shown in (F). The reduction in intensity for sub-resolution tubules is apparent. (G) shows the performance of the three different estimates of tubule width. The 50% distance measure (o) and the maximum gradient granulometry (square) perform well above about twice the psf, but return a value close to the psf for sub-resolution objects. The integrated intensity measure (x) gives a near linear response throughout the range of tubule widths examined. Similar result are obtained using a faster granulometry method that includes decomposition of the circular structuring element into linear approximations, along with an empirical correction of -1 pixel to compensate for oversampling (H).

from $FWHM_{min}$ in blue to $FWHM_{max}$ in red (Fig. 6.2 (a)).

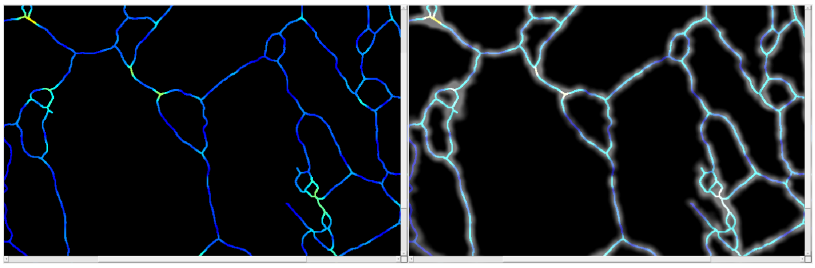

(a) Pseudo-color coded width (b) Width skeleton superimposed on the filtered image

Figure 6.2: Pseudo-colour coded representation of the tubule width (a) ranging from blue ($FWHM_{min}$) to red ($FWHM_{max}$). (b) Result of blending the width image with the filtered image to visually inspect the performance of the overall segmentation and width analysis method

The skeleton can also be superimposed on any other image, such as the filtered image (Fig. 6.2 (b)), using the merge dropdown menu, and the *'blend'* option as the **merge method** in the **Display controls** panel (Fig. 6.3). The **Toggle merge** button can be used to switch between a single image, defined by the **image** dropdown menu and the merged image (defined by the **merge** dropdown menu).

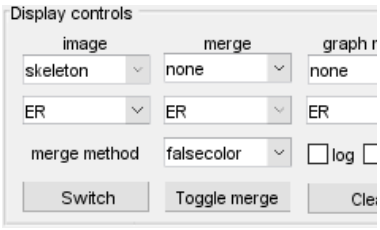

Figure 6.3: Controls used to merge the colour-coded skeleton with the filtered image

The identity of the two images can be reversed using the **Switch** button. The method used to compare the two images can be selected from:

- *'falsecolor'* : the first image is shown in magenta and the merge image is shown in green
- *'blend'* : The two images are alpha-blended retaining their original colors, but at 50% transparency.
- *'diff'* : the difference between the two images is displayed
- *'montage'* : the two images are shown side-by-side

6.2 *Conversion of the pixel skeleton to a graph representation*

The **analysis** button will calculate the width measurements and all subsequent steps to convert the pixel-skeleton to a weighted graph representation. For the tubular regions of the skeleton, the nodes are defined at the junctions between the ER tubules, or the end-points of free tubules, which are connected by straight edges that preserve the topology of the network (Fig. **??**). A number of metrics are associated with each edge including the Euclidean length of the underlying pixel skeleton, the average width calculated using each of the three methods, and the average width of the tubule excluding the nodes (termed *'center width'*), which provides a more accurate measure of the tubule diameter itself.

If any ER cisternae have been identified, they are represented as a 'super-node' positioned at the intensity-weighted centroid position that is connected to all the tubules that are incident on the feature boundary. Each of these tubes is given an arbitrary value

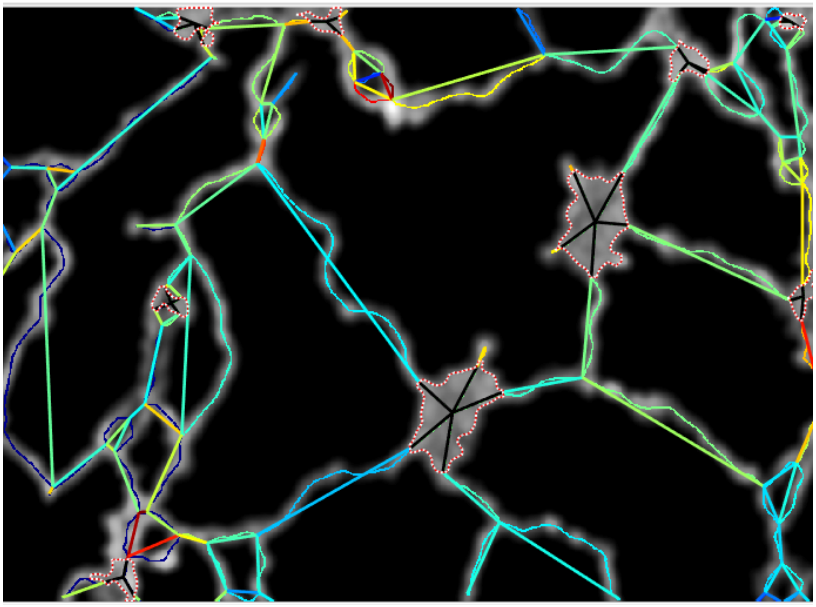

Figure 6.4: Conversion of the weighted pixel skeleton to a weighted graph. Junctions and free ends are represented as nodes linked by edges that have a vector of properties associated with them including width and length. Cisternae are represented as a 'super-node' connected to all the incident tubules on the boundary

equal to the average width value. The boundary of the cisternal features can be highlighted using the **plot feature** checkbox in the **Display controls** panel.

Once the weighted graph has been calculated, it is overlaid on the colour-coded pixel skeleton with the nodes at the junctions connected by straight edges that match the colour-coding of the skeleton. The **graph metric** displayed can be changed using the dropdown menu (Fig. 6.9), and the colour placed on a log scale by ticking the **log** checkbox. If the **scaled** checkbox is ticked the color-coded limits run from the min and max of the selected metric. If it is unchecked, the limits run between $FWHM_{min}$ and $FWHM_{max}$. The graph overlay can be removed by clicking the **Clear** button.

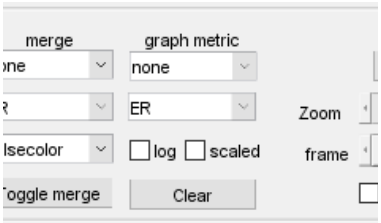

Figure 6.5: Controls used to select the graph metric to display

6.3 Tubule morphology

Under some conditions or in certain genetic backgrounds, such as over-expression of reticulons, the ER tubules show fluctuations in diameter along their length. The **Tubule morphology** panel can be used to charaterise the number, size and distribution of these bulges and constrictions (Fig. 6.3).

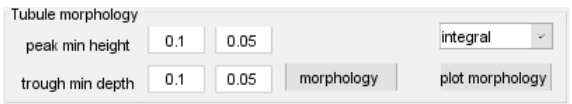

The pixel intensities are scanned along the length of each tubule starting at the nodes (which are set to 1), and the position and intensity of each peak that is greater than the **minimum peak height** and **minimum peak prominence** recorded (Fig. 6.6).

An additional minimum separation condition is imposed to

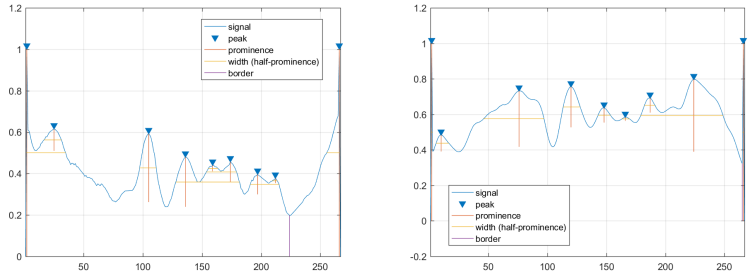

(a) detection of intensity peaks along an ER tubule

(b) detection of intensity troughs along an inverted ER profile

Figure 6.6: Tubule morphology: The intensity profile along each ER tubule is scanned to detect peaks above a minimum intensity that are also a minimum height above their neighbours. In addition peaks have to be greater than a minimum separation from each other and the nodes (set to one). (b) The position of the 'constrictions' between the peaks are determined from a scan of the inverted intensity profile

prevent noisy adjacent pixels from being considered as separate peaks and to exclude the original nodes from the analysis. This defaults to $FWHM_{min}$. A similar scan is used on the inverted tubule profile to detect the *'troughs'*. Once the location of the peaks and troughs has been determined, the width parameters at that point are extracted, along with the *separation* between the peaks.

The position and intensity value ot the bulges and constrictions are overlaid on the currently displayed image in green and red, respectively (Fig. 6.7). The metric plotted can be selected using the **plot morphology** dropdown menu (Fig. 6.3).

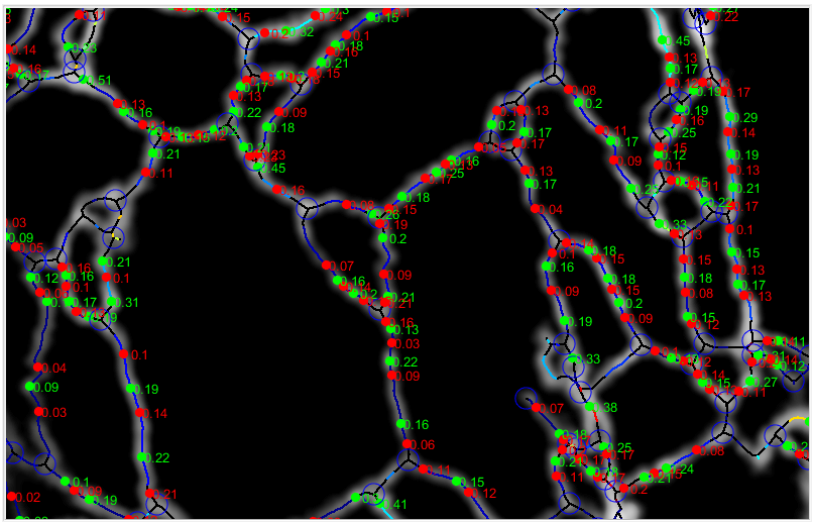

Figure 6.7: Measurement of bulges and constrictions in the ER network. The estimated width for every pixel in each edge is scanned to detect local peaks, corresponding to bulges (green) and troughs corresponding to constrictions (red), which are annotated with the estimate tubule width at that point

The summary results for all the tubules are shown in the **Results Summary** panel (Fig. 6.8 (a)), or plotted as histograms (Fig. 6.8 (b)).

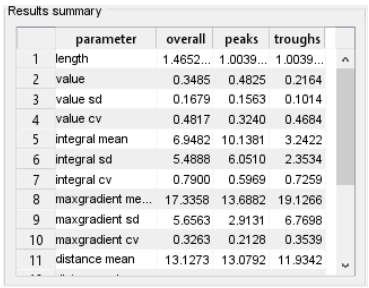

(a) Summary results for the tubule morphology measurements

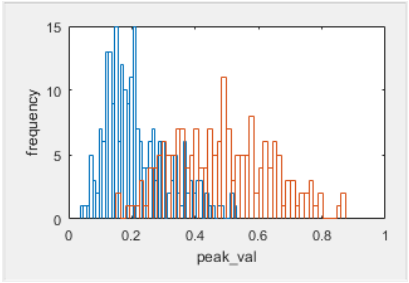

(b) Histogram plots for the peak and trough intensities

Figure 6.8: Tubule morphology results : (a) the average value, sd and cv for the the intensity and width estimates are shown for each entire tubule, and for the bulges and constrictions separately. (b) histogram display of the distribution of bulge and constriction intensities

6.4 Data output

The data and images from the analysis can be saved using the controls in the **Output** panel. The **Save image** button saves a version of the image currently displayed with all the annotations in '*.png' and '*.eps' format. The **Save data** button writes all the data on the ER tubules, ER cisternae, tubule morphology and polygonal regions to separate sheets in an Excel file. The **Panels** button saves a copy of the all the panels in the interface as '*.png' files that can be used to tailor the illustrations in this manual to any specific application.

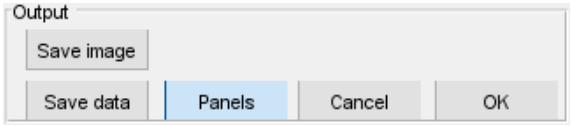

Figure 6.9: Output controls used to save data and images